# We are IntechOpen, the world's leading publisher of Open Access books Built by scientists, for scientists

**4,800**
Open access books available

**122,000**
International authors and editors

**135M**
Downloads

Our authors are among the

**154**
Countries delivered to

**TOP 1%**
most cited scientists

**12.2%**
Contributors from top 500 universities


WEB OF SCIENCE™

Selection of our books indexed in the Book Citation Index in Web of Science™ Core Collection (BKCI)

## Interested in publishing with us?
## Contact book.department@intechopen.com

Numbers displayed above are based on latest data collected.
For more information visit www.intechopen.com

# 11

# Wave Propagation in Elastic Media with Micro/Nano-Structures

G. L. Huang[1,3], C.T. Sun[2] and F. Song[3]
[1]*Department of Systems Engineering, University of Arkansas at Little Rock*
[2]*School of Aeronautics and Astronautics, Purdue University*
[3]*Department of Applied Science, University of Arkansas at Little Rock*
*USA*

## 1. Introduction

Micro- and nano-scale materials and structures such as plate- or beam-like structures with submicron or nano thicknesses have attracted considerable interest from the scientific community due to the increasingly strong demands of miniaturization in the fields of microelectronics and nanotechnology. More and more nano-structures, e.g. ultra-thin films, nanowires and nanotubes, have been fabricated and served as the basic building blocks for microelectromechanical systems (MEMS) and nanoelectromechanical systems (NEMS) (Jin et al., 1998; Craighead, 2000; Husain et al., 2003; Feng et al., 2007). For long-term stability and reliability of various devices at nanoscale, researchers should possess a deep understanding and knowledge of mechanical properties of nano materials and structures, especially for dynamic properties.

Among many techniques, high-frequency acoustic wave technique has been regarded as one of very efficient nondestructive methods to characterize elastic media with micro- or nano-structures. (Hernaandez et al., 2002) used high-frequency laser-excited guided acoustic waves to estimate the in-plane mechanical properties of silicon nitride membranes. Mechanical properties and residual stresses in the membranes were evaluated from measured acoustic dispersion curves. The mean values of the Young's modulus and density of three nanocrystalline diamond films and a free standing diamond plate were determined by analyzing the dispersion of laser-generated surface waves (Philip et al., 2003). Recently, growing interest of using terahertz (THz) waves in nanoscale materials and nano-photonic or nano-phononic devices has opened a new topic on the wave characteristics of nanomaterials (Schneider et al., 2000, Vollmannn et al., 2004; Ramprasad & Shi, 2005; Sampathkumar et al., 2006). As dimensions of the material become smaller, however, their resistance to deformation is increasingly determined by internal or external discontinuities (such as surfaces, grain boundary, strain gradient, and dislocation). Although many sophisticated approaches for predicting the mechanical properties of nanomaterials have been reported, few addressed the challenges posed by interior nanostructures such as the surfaces, interfaces, structural discontinuities and deformation gradient of the nanomaterials under extreme loading conditions. The use of atomistic simulation may be a potential solution in the long run. However, it is well known that the capability of this approach is

Source: Wave Propagation in Materials for Modern Applications, Book edited by: Andrey Petrin,
ISBN 978-953-7619-65-7, pp. 526, January 2010, INTECH, Croatia, downloaded from SCIYO.COM

much limited by its need of prohibitive computing time and an astronomical amount of data generated in the calculations.

It has been well recognized that classical continuum models become inadequate to describe the response of solids when the characteristic length (or wave length) of deformation becomes comparable to or smaller than the characteristic length of microstructures in the solid. The main reason for this deficiency of the classical continuum model can be attributed to its inability to account for the local motion of the microstructure. One common way to solve the above mentioned problem is to employ additional kinematic variables to describe the nonhomogeneous local deformation in the micro- or nano- structure of the solid. This approach leads to Cosserat continuum models (Cosserat & Cosserat, 1909) or micropolar models (Mindlin, 1964) or the like (Achenbach et al., 1968). However, the large number of material constants were left undetermined, which would require rather prohibitive experiments. Recently, (Chen & Lee, 2003a,b) have attempted to determine the material constants in the micromorphic theory (Eringen, 1999) by relating the micromorphic theory to atomistic models. To overcome those challenges, another approach toward developing a high order continuum theory was taken by considering the exact local configurations of the media. By employing several kinematic variables to describe the local motion in addition to the macro kinematic variables, the microstructure continuum theory was derived (Sun et al., 1968; Huang & Sun, 2006a,b, 2007, 2008; Huang & Song, 2008) for periodically layered and ealstic media with nanostructures. The main advantage of the approach is that the microstctural material constants can be obtained directly from the original material system without ambiguity.

The presence of surface stresses is another challenge of understanding the mechanical and physical properties of nanostructures espectially for such nanostructures that have small size and thus large surface area to volume (SAV) ratio. Much effort has been made to understand surface stress effects on the dynamic behavior of nanowires. Using the newly-developed surface Cauchy-Born model, (Park & Klein 2008) analyzed the surface stress effects on the nanowire resonant frequencies for varying boundary conditions. It was observed that if finite deformation kinematics are considered, the strain independent surface stresses will substantially alter the resonant frequencies of the nanowires. Wu and Dzenis (2006) investigated the longitudinal and flexural wave propagation in nanowires/fibers within the framework of conventional continuum mechanics. In the study, the surface effects were considered by introducing the strain-independent surface tension/stress in the conventional love's rod theory and Timoshenko beam theory. However, in those approaches, heterogeneous nanostructure effects upon the wave propagation in the nanowire were not considered. It should be mentioned that the heterogeneous nanostructure effects should be addressed when the characteristic length of deformation (or wave-length) becomes comparable to or smaller than the characteristic length of the heterogeneous nanostructures. Therefore, to capture heterogeneity of the nanowires for high frequency nanowire-based devices, (Song et al., 2009; Song & Huang, 2009) developed a high-order continuum model to study the surface stress influences on high-frequency longitudinal and flexural wave propagation in nanowires, from which the size dependent wave information were also observed. In the proposed model, additional kinematic variables were introduced to account for the nanostructure heterogeneity and the local motion in the nanowires. Surface effects were first incorporated into the current model by using the incremental deformation approach (Biot, 1965; Sun, 1972). The equations of motion including both strain-independent and –dependant surface stress effects were derived for

longitudinal and flexural wave motion. Some new physical wave phenomena related to the surface stress effects were analyzed and discussed.

The objective of this chapter is to introduce the microstructure continuum theory to study the wave propagation in elastic media with different micro- or nano- structures. First, wave propagation in the one-dimensional nanophononic crystal heterostructure will be investigated when the frequency is in range of THz. It is found that the current theory can give very good prediction of wave dispersion in nonphononic crystal structures. Then, the microstructure continuum theory will be used to study the high-frequency wave propagation in the two-dimensional ultra-thin films. The nanostructural effects upon the wave propagation in ultra-thin films are investigated. Both the in-plane and out-of-plane waves are considered. Finally, surface stress effects on dynamic begavior of nanowires are studied by using the new-developed high-order continuum theory.

## 2. Wave propagation in nanophononic crystal heterostrucutre

In this section, we introduce the microstrucuture continuum model to study wave propagation in a one-dimensional nanophononic crystal heterostructure. For simplicity, the heterostrucutre is represented by a one-dimensional lattice model system. We employ the microstructure continuum model to describe the mechanical behavior of the discrete lattice system. The accuracy of the microstructure continuum model is examined. Rather than the transverse wave as considered by (Ramprasad & Shi, 2005), the longitudinal wave propagation is investigated.

### 2.1 Microstructure continuum model for one-dimensional nanostructures

Consider a discrete heterostructure system consisting of two alternating layers of two different materials as shown in Fig. 1 (a). It is assumed that the material (material 1) in the first layer is comprised of a number of unit cells of atoms each consisting of two masses $m_1$ and $m_2$ (Fig. 1(a) only shows one unit cell in the each layer). Similarly, the unit cell in the other layer consists of masses $m_3$ and $m_4$. The pairwise interactions within each cell are represented by elastic springs with spring constants $k_1$, $k_2$ , $k_3$ and $k_4$, respectively, as shown in Fig. 1(a). The lattice constant between adjacent masses is denoted by $a$. It should be noted that the pairwise interaction parameters $k_2$ and $k_4$ are different from those in the corresponding bulk materials, since the interaction effects between different layers are assumed to be included in these parameters. However, it should be noted that the thickness of the interfacial layer between the two materials is neglected in this study.

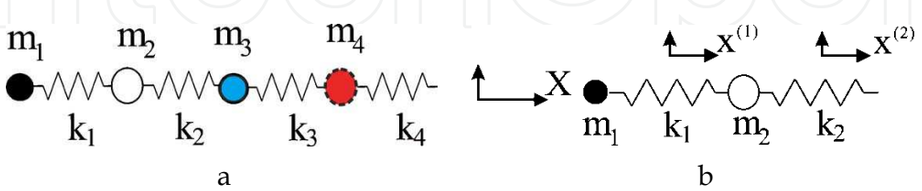


Fig. 1. (a) The lattice system for a nanophononic crystal with two-layered strucuture, and each layer has one unit cell consisting of two atoms. (b) The unit cell of material in layer 1

A microstructure continuum model is now developed to study longitudinal harmonic wave propagation in the nano heterostructure. A unit cell in layer 1 is shown in Fig. 1(b), where $x^{(1)}$ and $x^{(2)}$ indicate the local coordinate axes and $X$ the macro coordinate axis. It is noted

that the origin of the local coordinate system is located at the mid-point between the two masses. The local displacement fields in the two sub-regions in the unit cell are approximated by the global kinematic variables as

$$u^{(1)}(x^{(1)},X)=U\ (X)+\phi^{(1)}(X)x^{(1)},\quad u^{(2)}(x^{(2)},X)=U\ \left(X+a\right)+\phi^{(2)}(X)x^{(2)} \tag{1}$$

where $u^{(1)}(x^{(1)},X)$ and $u^{(2)}(x^{(2)},X)$ are the local displacements in the two sub-regions, and the global displacement $U$ and the kinematic variables $\phi^{(i)}(i=1,2)$ are functions of the global coordinate variable $X$. By using the continuity condition, $u^{(1)}(a/2,X)=u^{(2)}(-a/2,X)$, $\phi^{(2)}$ can be eliminated. From these approximate displacements given by Eq. (1), we can obtain the strain energy and kinetic energy densities, respectively, for the equivalent continuum:

$$W=\frac{1}{2a}\left[\frac{k_1}{2}(a\Phi)^2+\frac{k_2}{2}(2a\frac{\partial U}{\partial X}-a\Phi)^2\right] \tag{2}$$

and

$$T=\frac{1}{2a}\left[\frac{m_1}{2}(\dot{U}-\frac{a}{2}\dot{\Phi})^2+\frac{m_2}{2}(\dot{U}+\frac{a}{2}\dot{\Phi})^2\right] \tag{3}$$

where $\Phi\equiv\phi^{(1)}$. Subsequently, by using the Hamilton's principle (Achenbach, 1973), the equations of motion for the microstructure continuum medium are obtained as

$$\left(m_1+m_2\right)\ddot{U}-\frac{a}{2}\left(m_1-m_2\right)\ddot{\Phi}=k_2\left(4a^2\frac{\partial^2 U}{\partial X^2}-2a^2\frac{\partial\Phi}{\partial X}\right) \tag{4}$$

$$\frac{a^2}{4}\left(m_1+m_2\right)\ddot{\Phi}-\frac{a}{2}\left(m_1-m_2\right)\ddot{U}\ =-(k_1+k_2)a^2\Phi+2k_2a^2\frac{\partial U}{\partial X} \tag{5}$$

with the stress boundary condition along $X$ direction,

$$t\ =2k_2a\frac{\partial U}{\partial X}-k_2a\Phi \tag{6}$$

where $t$ is traction at the boundary. Eqs. (2)-(6) give a nonconventional continuum model with microstructure which is used to provide a better representation of the discrete lattice system.

The microstructure continuum model for layer 2 with one unit cell can be obtained by replacing $m_1$ and $m_2$ with $m_3$ and $m_4$, and $k_1$ and $k_2$ with $k_3$ and $k_4$, respectively. The equations of motion for the classical continuum model that represents this discrete system can be derived by ignoring microstructure effects. We have

$$k\frac{\partial^2 U}{\partial X^2}=\rho_0\ddot{U} \tag{7}$$

where $k\equiv 2ak_1k_2/\left(k_1+k_2\right)$ and $\rho_0\equiv\left(m_1+m_2\right)/\left(2a\right)$, from which the phase velocity of the representative classical continuum medium can be obtained as $c_0=2a\sqrt{\left(k_1k_2\right)/\left(k_1+k_2\right)\left(m_1+m_2\right)}$.

### 2.2 Numerical simulation

The accuracy of the microstructure continuum model for material 1 as described by Eqs. (2) and (3) or equivalently by Eqs. (4) and (5) can be evaluated by studying harmonic wave propagation in material 1 of infinite extent. Basically, this material is composed of identical unit cells shown in Fig. 1(b). Fig. 2(a) shows the comparison of the lowest dispersion curves (the acoustic mode) plotted with nondimensional phase velocity $c^*=c_p/c_0$ vs nondimensional wave number KL for $m_2/m_1$=0.4, $k_2/k_1$=0.5. The solution (labeled as "micro structure model") for the microstructure continuum model is obtained by assuming the wave form $U = A_1 e^{iK(X-c_p t)}$, $\Phi = A_2 e^{iK(X-c_p t)}$, where $K$ and $c_p$ denote wave number and phase velocity, respectively. The curve labeled as "exact solution" is calculated based on the discrete lattice system (Huang & Sun, 2006b). It is found that the micro structure continuum model is reasonably accurate for predicting wave dispersion at least up to KL=1.5. In contrast, the classical continuum model predicts a nondispersive behavior.

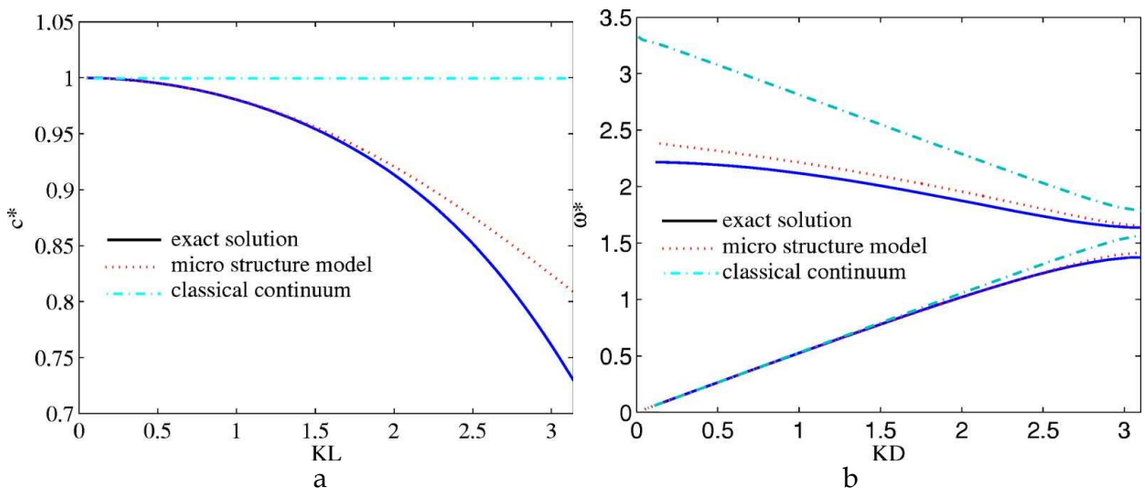


Fig. 2. (a) Comparison of the dispersive curves for bulk material one obtained with the lattice model and the microstructure continuum model ($L$ =2$a$). (b) Comparison of the dispersive curves for nanophononic crystal obtained with the lattice model, the microstructure continuum model, and classical continuum model ($D$ =4$a$)

Consider now longitudinal wave propagation in the nano-phononic structure consisting of alternating layers of materials 1 and 2 as shown in Fig. 1(a). Each layer has only one unit cell. Based on the microstructure continuum model, the two discrete layers of materials 1 and 2 can be represented by the respective continua with microstructures. The resulting system is a layered medium of two alternating layers of materials 1 and 2, respectively. Dispersion curves for longitudinal wave propagating though this layered medium can be solved using the Floquet theory (Sun et al., 1968). The numerical result for nondimensional angular frequency $\omega^* = \omega / \omega_0$, with $\omega = Kc_p$, $\omega_0 = c_0 / D$ and $D = 4a$, vs nondimensional wave number $KD$ as shown in Fig. 2(b) is obtained using the following material properties for the discrete nano-phononic system: $m_2/m_1$=0.4, $m_3/m_1$=0.6, $m_4/m_1$=0.3, $k_2/k_1$=0.5, $k_3/k_1$=0.5 and $k_4/k_2$=2.2. The ratio of the densities for the two materials is $\rho_1/\rho_2 = (m_1 + m_2)/(m_3 + m_4) = 0.64$. These material properties are selected to match those considered by (Ramprasad & Shi, 2005). For the purpose of comparison, the dispersion curves for the nano-phononic crystal obtained from the full discrete lattice system (labeled

as "exact solution") and from the classical continuum model are also shown in Fig. 2(b). It is evident that the present microstructure continuum model yields an almost perfect prediction for the acoustic mode and a very reasonable prediction for the optic mode. On the other hand, the classical continuum model is much less accurate especially for shorter wavelengths and for the optic mode.

In summary, this investigation has demonstrated that the microstructure continuum model can be used to describe with excellent accuracy wave propagation in nano-phononic crystals. It is also concluded that the conventional continuum model is adequate for certain heterostructures in which the dimensions of the constituent materials are large relative to those of the unit cells.

## 3. Wave propagation in ultra-thin films

In this section, we employ a procedure to develop a microstructure continuum model with microstructures based on the atomic structure of the ultra-thin film. The atomistic crystal structure of the thin film, for the sake of simplicity, is represented by a lattice model. The dimensions of the crystal structure naturally appear in the constitutive equations and the equations of motion of the representative continuum. The accuracy of the present model is evaluated by comparing dispersions of free harmonic waves predicted by the continuum model and exact analysis based on the lattice model.

### 3.1 Microstructure continuum model for ultra-thin films

A thin film of cubic structure as shown in Fig. 3 is considered. The thin film has a uniform thickness h and is assumed to be in a state of plane strain parallel to the $X_1$-$X_3$ plane. The discrete solid dots denote atoms $m_1$ and $m_2$. The spacing between two adjacent atoms is $a$. Only the interactions between the nearest and next-nearest neighbors are considered. By assuming infinitesimal deformations, the interactions are represented by linearly elastic springs with spring constants $\alpha_1$ and $\alpha_2$, respectively (Ghatak et al., 1972). Although the cubic structure is chosen for the sake of mathematical simplicity, the proposed approach can be readily applied for thin films with other crystal structures.

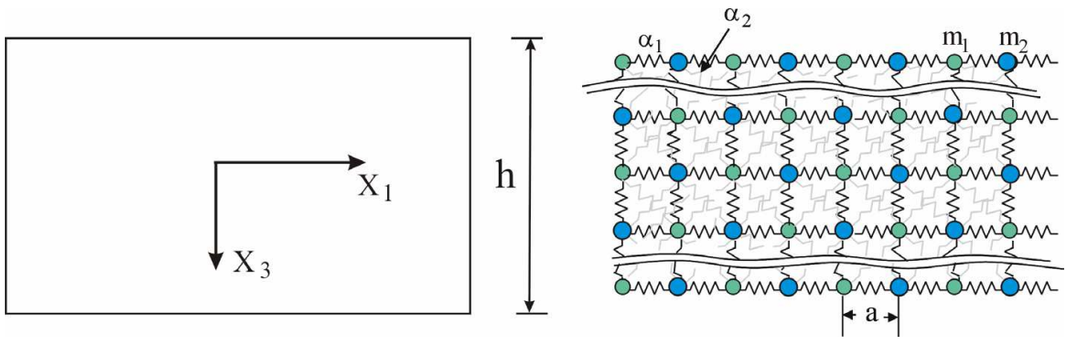


Fig. 3. Thin film structure and its lattice system

A representative unit cell (see Fig. 4) of the cubic lattice model is considered in this study. The representative cell is composed of four sub-cells. In each subcell, a local coordinate system is set up as shown in Fig. 4. Note that in this representative element, atoms 3, 6, 7, 8, and 9 are not included in the representative cell because they are included in the adjacent cells. The four local coordinate systems $(x_1^{(k)}, x_3^{(k)})$ with origins located at the geometrical

centers of the four sub-cells ($k$ = 1-4), respectively, are set up so that $x_1$ and $x_3$ are parallel to the global (macro) coordinates $X_1$ and $X_3$, respectively.

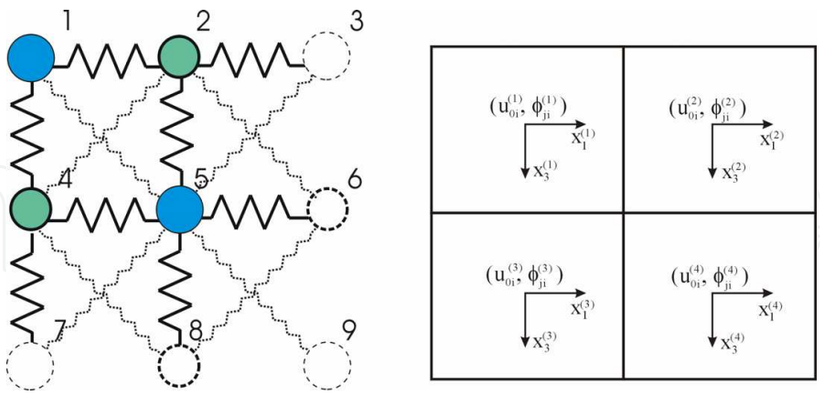


Fig. 4. Representative unit cell and the equivalent continuum

The local displacements $u_i^{(k)}$ in each sub-element are expanded in power series with respect to the respective local coordinates as

$$u_i^{(k)} = u_{0i}^{(k)} + \phi_{1i}^{(k)} x_1^{(k)} + \phi_{3i}^{(k)} x_3^{(k)}, \; k = 1, 2, 3, 4 \tag{8}$$

where the expansion is truncated at the linear terms. Greater accuracy may be achieved by adding higher order terms in Eq. (8) (Huang & Sun, 2008). We assume that local translational displacements $u_{0i}^{(k)}$ of the four sub-cells are values of macro-displacement $U_i$ at the four sub-cells, respectively, i.e.,

$$\begin{aligned}
&u_{0i}^{(1)}(X_1, X_3) = U_i(X_1, X_3), \\
&u_{0i}^{(2)} = U_i(X_1 + a, X_3) \approx U_i(X_1, X_3) + a\frac{\partial U_i}{\partial X_1}, \\
&u_{0i}^{(3)} = U_i(X_1, X_3 + a) \approx U_i(X_1, X_3) + a\frac{\partial U_i}{\partial X_3}, \\
&u_{0i}^{(4)} = U_i(X_1 + a, X_3 + a) \approx U_i(X_1, X_3) + a\frac{\partial U_i}{\partial X_1} + a\frac{\partial U_i}{\partial X_3}
\end{aligned} \tag{9}$$

The kinematic variables $u_{0i}^{(k)}, \phi_{1i}^{(k)}$ and $\phi_{1i}^{(k)}$ are required to satisfy the displacement continuity conditions along the boundaries shared by the adjacent pairs of the sub-cells. These boundary conditions lead to the following relations:

$$[\phi_{ji}^{(2)}] = \begin{bmatrix} 2\dfrac{\partial U_1}{\partial X_1} - \Phi_{11} & 2\dfrac{\partial U_3}{\partial X_1} - \Phi_{13} \\ \Phi_{31} & \Phi_{33} \end{bmatrix} \tag{10}$$

$$[\phi_{ji}^{(3)}] = \begin{bmatrix} \Phi_{11} & \Phi_{13} \\ 2\dfrac{\partial U_1}{\partial X_3} - \Phi_{31} & 2\dfrac{\partial U_3}{\partial X_3} - \Phi_{33} \end{bmatrix} \tag{11}$$

$$[\phi_{ji}^{(4)}]=\begin{bmatrix} 2\dfrac{\partial U_1}{\partial X_1}-\Phi_{11} & 2\dfrac{\partial U_3}{\partial X_1}-\Phi_{13} \\ 2\dfrac{\partial U_1}{\partial X_3}-\Phi_{31} & 2\dfrac{\partial U_3}{\partial X_3}-\Phi_{33} \end{bmatrix} \tag{12}$$

in which

$$\Phi_{ji}(X_1,X_3)\equiv\phi_{ji}^{(1)}(X_1,X_3) \tag{13}$$

The deformation energy in each sub-cell can be written as

$$W^{(1)}=W_{1-2}+W_{1-4}+W_{1-5}+W_{2-4} \tag{14}$$

$$W^{(2)}=W_{2-3}+W_{2-5}+W_{2-6}+W_{3-5} \tag{15}$$

$$W^{(3)}=W_{4-5}+W_{4-7}+W_{4-8}+W_{5-7} \tag{16}$$

where superscripts 1, 2, 3, and 4 represent the sub-cells, and $W_{1-2}$, $W_{1-5}\cdots$ denote the total deformation energies due to stretching of the springs between atoms 1 and 2, and 1 and5..., respectively. The total deformation energy in sub-cell 1 is

$$W^{(1)}=\frac{1}{2}\alpha_1 a^2\left[\left(\phi_{11}^{(1)}\right)^2+\left(\phi_{33}^{(1)}\right)^2\right]+\frac{1}{4}\alpha_2\left(\phi_{11}^{(1)}+\phi_{31}^{(1)}+\phi_{13}^{(1)}+\phi_{33}^{(1)}\right)^2+\frac{1}{4}\alpha_2\left(\phi_{11}^{(1)}-\phi_{31}^{(1)}-\phi_{13}^{(1)}+\phi_{33}^{(1)}\right)^2 \tag{18}$$

The deformation energies for other sub-cells have a similar expression as Eq. (18).

Based on the continuity conditions of displacements, Eqs. (10)-(12), the kinematic variables $\phi_{ji}^{(k)}(j,i=2,3,4)$ in sub-cells 2, 3, and 4 can be eliminated and expressed in terms of the kinematic variables of sub-cell 1. Thus, the total deformation energy stored in the representative unit cell (that consists of 4 sub-cells) can be expressed in terms of $U_i$ and $\Phi_{ji}$ and their derivatives. By dividing this total energy with the planar area $4a^2$, we obtain the strain energy density $W$ of the representative cell after some manipulations. We have

$$\begin{aligned} W&=\frac{1}{4a^2}\left(W^{(1)}+W^{(2)}+W^{(3)}+W^{(4)}\right) \\ &=\frac{1}{2}\alpha_1(E_{11}^2+E_{33}^2+\gamma_{11}^2+\gamma_{33}^2)+\frac{1}{2}\alpha_2\left[\left(E_{11}+E_{33}\right)^2+\gamma_{11}^2+\gamma_{33}^2+\gamma_{13}^2+\gamma_{31}^2+4E_{13}^2\right] \end{aligned} \tag{19}$$

where

$$E_{ij}=\frac{1}{2}\left(U_{i,j}+U_{j,i}\right),\quad i,j=1,3 \tag{20}$$

is the macro strain and

$$\gamma_{ji}=U_{j,i}-\Phi_{ji},\ i,j=1,3 \tag{21}$$

is the relative strain. These two deformation variables resemble those in Mindlin's microstructure theory (Mindlin, 1964). This strain energy density function forms the base of the continuum model that represents the discrete lattice system.

To establish the constitutive relations we define Cauchy stress and relative stress, respectively

$$\Sigma_{ij} = \frac{\partial W}{\partial E_{ij}} \tag{22}$$

$$\sigma_{ij}^{R} = \frac{\partial W}{\partial \gamma_{ij}} \tag{23}$$

It is noted that if $\gamma_{ij}$ is absent, then the relative stress $\sigma_{ij}^{R}$ vanishes, and the strain energy density function reduces to that of the classical continuum. This reduced model will be referred to as the "effective modulus" theory.

The kinetic energy density function for the representative cell of the thin film can be derived from the discrete system based on the local displacements given by Eq. (8). We obtain

$$\begin{aligned} T = {} & \frac{m_1}{4a^2}\left[\dot{U}_1^2 + \dot{U}_3^2 + \frac{a^2}{4}\left(\dot{\Phi}_{11} + \dot{\Phi}_{31}\right)^2 + \frac{a^2}{4}\left(\dot{\Phi}_{13} + \dot{\Phi}_{33}\right)^2\right] + \\ & \frac{m_2}{4a^2}\left[\dot{U}_1^2 + \dot{U}_3^2 + \frac{a^2}{4}\left(\dot{\Phi}_{11} - \dot{\Phi}_{31}\right)^2 + \frac{a^2}{4}\left(\dot{\Phi}_{13} - \dot{\Phi}_{33}\right)^2\right] \end{aligned} \tag{24}$$

where a dot represents the derivative with respect to time.

To complete the continuum model, the Hamilton's principle is conducted to obtain the equations of motion:

$$\begin{aligned} & -\frac{1}{2a^2}(m_1 + m_2)\ddot{U}_1 + \alpha_1\left(2\frac{\partial^2 U_1}{\partial X_1^{\,2}} - \frac{\partial \Phi_{11}}{\partial X_1}\right) \\ & +\alpha_2\left(2\frac{\partial^2 U_1}{\partial X_1^{\,2}} + 2\frac{\partial^2 U_1}{\partial X_3^{\,2}} + 2\frac{\partial^2 U_3}{\partial X_1 \partial X_3} - \frac{\partial \Phi_{11}}{\partial X_1} - \frac{\partial \Phi_{31}}{\partial X_3}\right) = 0 \end{aligned} \tag{25}$$

$$\begin{aligned} & -\frac{1}{2a^2}(m_1 + m_2)\ddot{U}_3 + \alpha_1\left(2\frac{\partial^2 U_3}{\partial X_1^{\,2}} - \frac{\partial \Phi_{33}}{\partial X_3}\right) \\ & +\alpha_2\left(2\frac{\partial^2 U_3}{\partial X_1^{\,2}} + 2\frac{\partial^2 U_3}{\partial X_3^{\,2}} + 2\frac{\partial^2 U_1}{\partial X_1 \partial X_3} - \frac{\partial \Phi_{13}}{\partial X_1} - \frac{\partial \Phi_{33}}{\partial X_3}\right) = 0 \end{aligned} \tag{26}$$

$$\frac{1}{8}(m_1 + m_2)\ddot{\Phi}_{11} + \frac{1}{8}(m_1 - m_2)\ddot{\Phi}_{31} + (\alpha_1 + \alpha_2)\left(\Phi_{11} - \frac{\partial U_1}{\partial X_1}\right) = 0 \tag{27}$$

$$\frac{1}{8}(m_1 + m_2)\ddot{\Phi}_{33} + \frac{1}{8}(m_1 - m_2)\ddot{\Phi}_{13} + (\alpha_1 + \alpha_2)\left(\Phi_{33} - \frac{\partial U_3}{\partial X_3}\right) = 0 \tag{28}$$

$$\frac{1}{8}(m_1+m_2)\ddot{\Phi}_{31}+\frac{1}{8}(m_1-m_2)\ddot{\Phi}_{11}+\alpha_2\left(\Phi_{31}-\frac{\partial U_1}{\partial X_3}\right)=0 \tag{29}$$

$$\frac{1}{8}(m_1+m_2)\ddot{\Phi}_{13}+\frac{1}{8}(m_1-m_2)\ddot{\Phi}_{33}+\alpha_2\left(\Phi_{13}-\frac{\partial U_3}{\partial X_1}\right)=0 \tag{30}$$

The boundary conditions are

$$T_j=\left(\Sigma_{ji}+\sigma_{ji}^R\right)n_i\,,\ P_{ji}=0 \tag{31}$$

where $n_i$ the unit vector normal to the boundary surface, $T_i$ is external traction, and $P_{ji}$ the external couple. It is noted that, for present continuum model developed based on the linear displacement expansion of Eq. (8), no couple stress is present.

The equations of motion for the reduced effective modulus theory are readily obtained by requiring $\gamma_{ij}=0$ in the energy density function. We have

$$\alpha_1\frac{\partial^2 U_1}{\partial {X_1}^2}+\alpha_2\left(\frac{\partial^2 U_1}{\partial {X_1}^2}+\frac{\partial^2 U_1}{\partial {X_3}^2}+2\frac{\partial^2 U_3}{\partial X_1\partial X_3}\right)=\frac{1}{2a^2}(m_1+m_2)\ddot{U}_1 \tag{32}$$

$$\alpha_1\frac{\partial^2 U_3}{\partial {X_1}^2}+\alpha_2\left(\frac{\partial^2 U_3}{\partial {X_1}^2}+\frac{\partial^2 U_3}{\partial {X_3}^2}+2\frac{\partial^2 U_1}{\partial X_1\partial X_3}\right)=\frac{1}{2a^2}(m_1+m_2)\ddot{U}_3 \tag{33}$$

### 3.2 Wave propagation

The continuum theory with microstructures previously presented is now employed to study propagation of harmonic waves in a thin film of thickness $h$ and of infinite in-plane dimensions. The thin film is assumed to consist of a number of atom layers, and the surfaces $X_3=\pm h/2$ are free of tractions. Harmonic waves propagating in the $X_1$-direction can be expressed as

$$U_1=f_1(X_3)e^{ik(X_1-ct)}\,,\ U_3=f_2(X_3)e^{ik(X_1-ct)} \tag{34}$$

$$\Phi_{11}=f_3(X_3)e^{ik(X_1-ct)}\,,\ \Phi_{33}=f_4(X_3)e^{ik(X_1-ct)} \tag{35}$$

$$\Phi_{31}=f_5(X_3)e^{ik(X_1-ct)}\,,\ \Phi_{13}=f_6(X_3)e^{ik(X_1-ct)} \tag{36}$$

where $k$ denotes wave number, $c$ is phase velocity, and $f_i(X_3)$ are unknown functions. Substituting Eqs. (34)-(36) in the equations of motion (25)-(30), and eliminating $f_2$, $f_3$, $f_4$, $f_5$, and $f_6$, we obtain

$$\begin{aligned}&C_1C_5f_1''''+(C_5C_2+C_6C_1)f_1'''-(C_4C_8-C_5C_3-C_6C_2-C_1C_7)f_1''\\&+(C_3C_6+C_2C_7)f_1'+C_7C_3f_1=0\end{aligned} \tag{37}$$

where

$$C_1 = (2 - D_8)\alpha_2\,,\ C_2 = -ik(\alpha_1 + \alpha_2)D_2 - \alpha_2 D_7$$

$$C_3 = \frac{\omega^2}{2a^2}(m_1 + m_2) - 2k^2(\alpha_1 + \alpha_2) - ik(\alpha_1 + \alpha_2)D_1$$

$$C_4 = C_8 = 2ik\alpha_2\,,\ C_5 = (\alpha_1 + \alpha_2)(2 - D_4)$$

$$C_6 = -(\alpha_1 + \alpha_2)D_3 - ik\alpha_2 D_6\,,\ C_7 = \frac{\omega^2}{2a^2}(m_1 + m_2) - 2k^2\alpha_2 - ik\alpha_2 D_5$$

$$D_1 = -ik(\alpha_1 + \alpha_2)\left[\frac{\omega^2}{2a^2}(m_1 + m_2) - \alpha_2\right],\ D_2 = \frac{\omega^2}{8a^2}(m_1 - m_2)\alpha_2$$

$$D_3 = ik\frac{\omega^2}{8a^2}(m_1 - m_2)\alpha_2\,,\ D_4 = -(\alpha_1 + \alpha_2)\left[\frac{\omega^2}{2a^2}(m_1 + m_2) - \alpha_2\right]$$

$$D_5 = -ik\alpha_2\left[\frac{\omega^2}{2a^2}(m_1 + m_2) - \alpha_1 - \alpha_2\right],\ D_6 = \frac{\omega^2}{8a^2}(m_1 - m_2)(\alpha_1 + \alpha_2)$$

$$D_7 = ik\frac{\omega^2}{8a^2}(m_1 - m_2)(\alpha_1 + \alpha_2)\,,\ D_8 = -\alpha_2\left[\frac{\omega^2}{2a^2}(m_1 + m_2) - \alpha_1 - \alpha_2\right]$$

The general solutions of Eq. (37) for the function $f_1$ depend on the type of the roots of the characteristic equation

$$\begin{aligned} &C_1C_5\beta^4 + (C_5C_2 + C_6C_1)\beta^3 - (C_4C_8 - C_5C_3 - C_6C_2 - C_1C_7)\beta^2 \\ &+(C_3C_6 + C_2C_7)\beta + C_7C_3 = 0 \end{aligned} \tag{38}$$

By solving the above biquadratic equation, the general solution for $f_1$ can be expressed as

$$f_1 = E_1 e^{\beta_1 X_3} + E_2 e^{\beta_2 X_3} + E_3 e^{\beta_3 X_3} + E_4 e^{\beta_4 X_3} \tag{39}$$

where $\beta_1$, $\beta_2$, $\beta_3$ and $\beta_4$ are the four roots of Eq. (38). The solutions for other functions $f_i$, $i$=2-6 can be obtained in a similar manner.

The traction-free boundary conditions at $X_3 = \pm h/2$ lead to

$$S_1E_1e^{(\beta_1 h/2)} + S_2E_2e^{(\beta_2 h/2)} + S_3E_3e^{(\beta_3 h/2)} + S_4E_4e^{(\beta_4 h/2)} = 0 \tag{40}$$

$$S_5E_1e^{(\beta_1 h/2)} + S_6E_2e^{(\beta_2 h/2)} + S_7E_3e^{(\beta_3 h/2)} + S_8E_4e^{(\beta_4 h/2)} = 0 \tag{41}$$

$$S_1E_1e^{(-\beta_1 h/2)} + S_2E_2e^{(-\beta_2 h/2)} + S_3E_3e^{(-\beta_3 h/2)} + S_4E_4e^{(-\beta_4 h/2)} = 0 \tag{42}$$

$$S_5E_1e^{(-\beta_1 h/2)} + S_6E_2e^{(-\beta_2 h/2)} + S_7E_3e^{(-\beta_3 h/2)} + S_8E_4e^{(-\beta_4 h/2)} = 0 \tag{43}$$

where

$$S_m = (2 - D_8)F_m + ikH_m - D_7\,,\ S_{m+4} = (\alpha_1 + \alpha_2)\left[(2 - D_4)H_m - D_3F_m\right] + ik\alpha_2$$

$$F_m = \beta_m^3 \frac{C_5C_1}{C_4C_7} - \beta_m \frac{C_8C_4 - C_5C_3}{C_4C_7}\,,\ H_m = -\frac{1}{C_4}\left(C_3 + \beta_m^2 C_1\right),\ m=1,2,3,4$$

Eqs. (40)-(43) have nontrivial solutions for $E_1$, $E_2$, $E_3$, and $E_4$ only if the determinant of the coefficients vanishes. This leads to the dispersion equation:

$$\begin{vmatrix} S_1e^{\beta_1 h/2} & S_2e^{\beta_2 h/2} & S_3e^{\beta_3 h/2} & S_4e^{\beta_4 h/2} \\ S_5e^{\beta_1 h/2} & S_6e^{\beta_2 h/2} & S_7e^{\beta_3 h/2} & S_8e^{\beta_4 h/2} \\ S_1e^{-\beta_1 h/2} & S_2e^{-\beta_2 h/2} & S_3e^{-\beta_3 h/2} & S_4e^{-\beta_4 h/2} \\ S_5e^{-\beta_1 h/2} & S_6e^{-\beta_2 h/2} & S_7e^{-\beta_3 h/2} & S_8e^{-\beta_4 h/2} \end{vmatrix} = 0 \tag{44}$$

Surface wave propagation and anti-plane wave propagation in ultra-thin films were investigated following a similar manner, and more details can be found in (Huang & Sun 2006a; Huang & Song, 2008), respectively.

### 3.3 Numerical simulation

Fig. 5 shows the comparison of dispersion curves for the lowest symmetric mode and anti-symmetric mode obtained according to Eq. (44) of the continuum model with microstructures, the effective modulus theory (Eqs. (32) and (33)), and the exact solution for the lattice system (Huang & Sun, 2006a), respectively. The parameters used in the calculation for the cubic crystal structure are $a = 1.74 \times 10^{-10} m$, $\alpha_1 = 2.02N/m$, $\alpha_2 = 1.10N/m$, $m_2/m_1 = 10$ and the film thickness is $h = 8a$ (i.e., 7 atom layers). The normalized wave velocity $c^* = c/\sqrt{\alpha_2/\rho_0}$, with $\rho_0 = (m_1 + m_2)/(2a^2)$, is used in the figure. The results of Fig. 5(a) clearly shows that both the effective modulus theory and the continuum model with microstructures yield very good predictions for the anti-symmetric wave for long waves with $ka$<0.5. This is expected because at lower frequencies wave dispersion is mainly caused by the finite thickness of the film and not by the effect of microstructures. However, as wave length decreases, the dispersion curve computed from the effective modulus theory deviates substantially from the exact curve, while the curve predicted by the continuum theory with microstructures is in good agreement with the exact curve. On the other hand if one employs the effective modulus theory and waves with $ka$>0.5 to determine elastic constants of a thin film with the aid of the dispersion relations, the values of these constants may be significantly overestimated.

Fig. 5 (b) shows the dispersion curves for the lowest symmetric mode. The dispersion curve predicted by the present continuum model with microstructures shows a better agreement with the exact solution than that by the effective modulus theory. It is of interest to note that the results by both continuum theories show some difference relative to the exact phase velocity at long wave lengths. This discrepancy is attributed to the fact both the present continuum theory and the effective modulus theory are not capable of accounting for the nano scale surface effect on the thin film. However, this surface effect can be neglected in thin films consisting of 20 or more atom layers (Sun & Zhang, 2003). Consequently, if one wants to use the lowest symmetric wave mode to determined thin film material properties, some data corrections should be exercised when the thickness of thin film is less than 6 - 7 nano-meters.

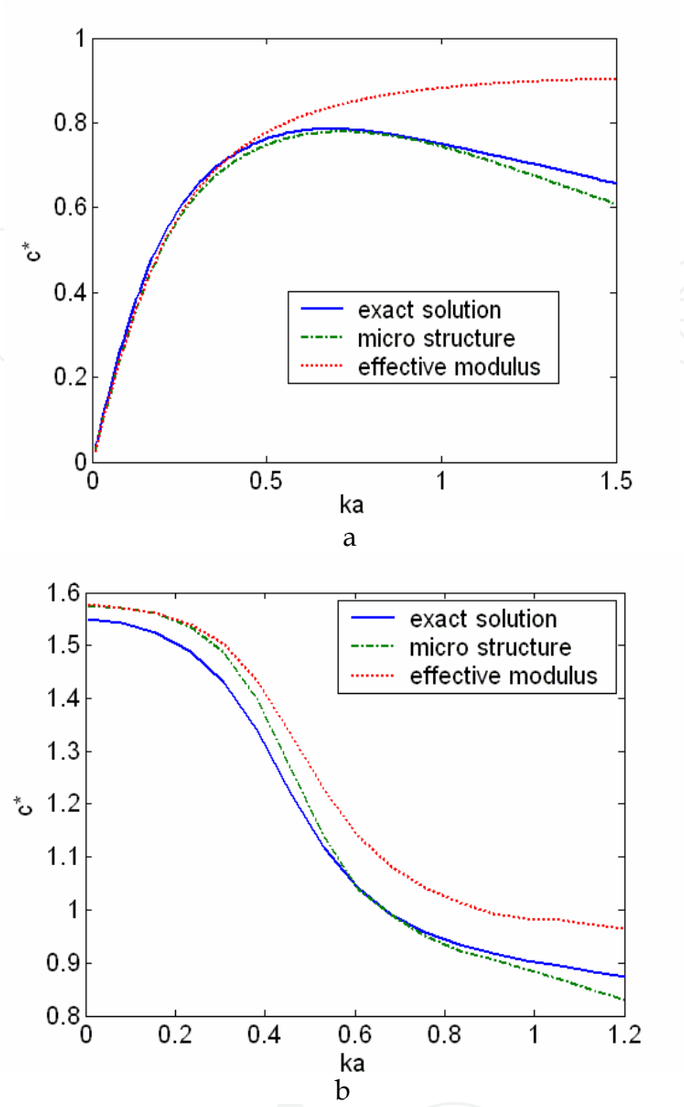


Fig. 5. Dispersive curves obtained with the lattice model and continuum models for a thin film with 7 atom layers. (a) Antisymmetric mode. (b) Symmetric mode

It is well known that in a classical elastic solid, the Rayleigh surface wave is nondispersive. However, surface waves with wavelengths that are comparable to the atomic spacing must be carefully examined if the surface wave technique is to be used in measuring material constants. It is noteworthy that, especially in electronic device applications, surface wave frequencies on the order of GHz -THz are now possible for this type of measurement. We now consider the two-dimensional problem of waves propagating along the surface of a semi-infinite continuum with microstructure as schematically shown in Fig. 6(a). This continuum is assumed to represent a material of the cubic structure and $X_1$-axis is parallel to the [100] crystal direction. The exact solution for surface waves in a half-space lattice can be refered to (Huang & Sun, 2006a) for the lattice system. To simulate the semi-infinite medium, lattice systems of 90 and 110 layers of atoms are both used with the bottom layer fixed. The results indicate that there is little difference between the two solutions.

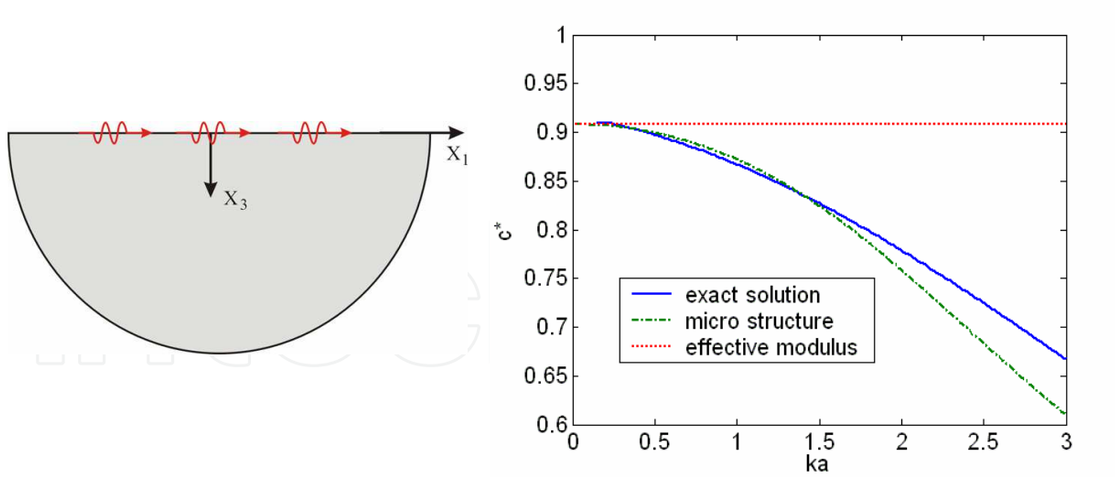


a b

Fig. 6. (a) Surface wave propagation in the generalized elastic medium. (b) Dispersive curves for surface waves obtained with the lattice model, the continuum theory with micro structures, and the effective modulus theory

Fig. 6(b) shows the dispersion curves for surface waves, effective modulus theory, and the corresponding lattice system, respectively. The parameters of the cubic crystal structure used in the calculations are $a = 1.74 \times 10^{-10} m$, $\alpha_1 = 2.02 N/m$, $\alpha_2 = 1.10 N/m$, $m_2/m_1 = 10$. For this set of material parameters, the roots are $\beta_1 = -4.2 \times 10^7 + 1.01 \times 10^7 i$ and $\beta_2 = -4.2 \times 10^7 - 1.01 \times 10^7 i$ for $ka$=0.015. The resulting displacement components in the $X_3$ direction are found to decay rapidly along the $X_3$ axis. The rate of decay depends on wave length. In general, the displacement components diminish within about two times the wave length. From Fig. 6(b), it is evident that, unlike the classical continuum, surface waves in the lattice system are dispersive and the present continuum model with microstructures describes this dispersive behavior pretty well. In contrast, the effective modulus theory fails to capture it. We have examined the validity in using the classical continuum (effective modulus) theory to analyze high frequency/short wavelength harmonic waves in thin films. It was observed that the effective modulus theory is inadequate for describing waves of short wavelengths propagating in thin films. It was also found that the continuum theory with microstructures provides much more accurate predictions of dispersive wave velocities of short wavelengths.

## 4. Wave propagation in nanowires with surface effects

To study high-frequency wave propagation in the nanowire with surface effects, a high-order continuum model is necessary and needed to capture heterogeneous nanostructure effects. In the model, additional kinematic variables are introduced to describe the local motion of nanostructures. Moreover, effects of the surface stress upon the wave propagation will be first considered by using the incremental deformation approach.

### 4.1 High-order continuum model for nanwires with surface effects

#### 4.1.1 Longitudinal wave motion

Consider first a longitudinal wave propagating in an elastic nanowire with constant circular cross section as illustrated in Fig. 7. A cylindrical coordinate system ($r$, $\theta$, $x$) is adopted with

the origin of the coordinate at the center of the cross section, where $r$, $\theta$, $x$ are the radial coordinate, azimuthal coordinate and longitudinal coordinate, respectively. In the figure, the symbol $\tau$ represents the surface stress acting along the axis direction of the nanowire, and $R$ denotes the radius of the nanowire.

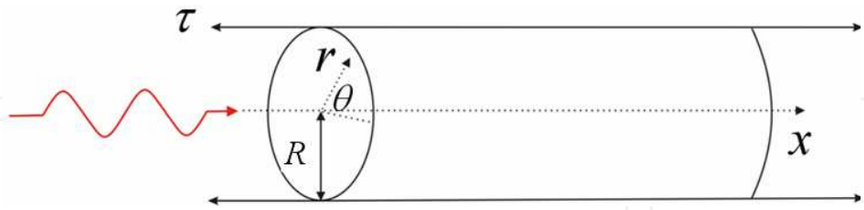


Fig. 7. Longitudinal wave propagation in the nanowire with uniform surface stresses

Based on the surface elasticity theory, the general linear constitutive relation of the surface can be written as

$$\tau_{ij} = \tau_0 \delta_{ij} + \lambda_s \varepsilon^s_{vv} \delta_{ij} + 2G_s \varepsilon^s_{ij} \tag{45}$$

where the subscripts ( $i$ and $j$) denote the stress and strain components along $r$, $\theta$ and $x$ directions, $\delta_{ij}$ denotes the Kronecker delta, repeated subscripts follow index summation, $\tau_{ij}$ represents the total surface stress, $\tau_0$ represents the strain-independent surface stress, $\varepsilon^s_{ij}$ is the surface strain, and $\lambda_s$ and $G_s$ denote surface moduli, respectively. For the longitudinal wave propagation problem, the constitutive relation of the surface stress can be simplified as

$$\tau = \tau_0 + \tau_e \tag{46}$$

where $\tau_e = (\lambda_s + 2G_s)\varepsilon^s_{xx} = E_s \varepsilon^s_{xx}$ is the strain -dependant stress, and $\varepsilon^s_{xx} = \varepsilon_{xx}\big|_{r=R}$.
To capture heterogeneous nanostructure effects, a generalized high-order continuum model is used to describe local displacements in the nanowire as

$$u_x = U_x(x,t),\ u_r = \xi_1(x,t) r + \xi_2(x,t) r^2 \tag{47}$$

where $u_x$ and $u_r$ are the local displacements in the longitudinal and radial directions respectively, and $\Phi_1(x,t)$ and $\Phi_2(x,t)$ are the kinematic variables to capture local motion due to the heterogeneity along radial direction. Based on Eq. (47), linearized local strain components can be obtained as

$$\begin{aligned} &\varepsilon_{xx} = \partial U_x(x,t)/\partial x,\ \varepsilon_{\theta\theta} = r\xi_1(x,t) + r\xi_2(x,t) \\ &\varepsilon_{rr} = r\xi_1(x,t) + 2r\xi_2(x,t) \end{aligned} \tag{48}$$

and the isotropic constitutive equations can be expressed as

$$\sigma_{xx} = \lambda(\varepsilon_{xx} + \varepsilon_{rr} + \varepsilon_{\theta\theta}) + 2G\varepsilon_{xx} \tag{49}$$

where $\lambda$ and $G$ are the Lame constants of the nanowire.
To consider surface stress $\tau$, the formulation according to Trefftz's theory will be taken (Biot, 1965; Sun, 1972). Using Trefftz's incremental stress components which are assumed to

be related linearly to the accompanying deformation, we can obtain an expression for the incremental strain energy density for the surface stressed nanowire as

$$\Delta U = \left\langle \int_0^{\varepsilon_{xx}} \sigma_{xx} d\varepsilon_{xx} + \int_0^{\varepsilon_{xx}} \tau_e d\varepsilon_{xx} + \int_0^{\hat{\varepsilon}_{xx}} \tau_0 d\hat{\varepsilon}_{xx} - \int_0^{\varepsilon_{xx}} \tau_0 d\varepsilon_{xx} \right\rangle \tag{50}$$

in which $\langle \cdot \rangle = \frac{1}{V}\int_V (\bullet) dV$ , $V$ is volume of the nanowire, and $\hat{\varepsilon}_{xx} = \frac{\partial u_x}{\partial x} + \frac{1}{2}\left(\frac{\partial u_x}{\partial x}\right)^2 + \frac{1}{2}\left(\frac{\partial u_r}{\partial x}\right)^2$ is the Lagrangian stain component.

The kinetic energy density for the longitudinal motion can be expressed by

$$T = \left\langle \frac{1}{2}\rho\left(\dot{u}_x^2 + \dot{u}_r^2\right) \right\rangle \tag{51}$$

where $\rho$ is the mass density of the nanowire.

By applying the Hamilton's principle, the equations of motion in the nanowire with surface stresses can be obtained as

$$\rho \ddot{U}_x - 2\lambda\left(\frac{\partial \xi_1}{\partial x} + R\frac{\partial \xi_2}{\partial x}\right) - \left[\lambda + 2G + (1-v)\frac{2\tau_0}{R} + \frac{2E_s}{R}\right]\frac{\partial^2 U_x}{\partial x^2} = 0 \tag{52}$$

$$\rho R^2 \ddot{\xi}_1 + \frac{4}{5}\rho R^3 \ddot{\xi}_2 + (8\lambda + 2G)(\xi_1 + R\xi_2) + 4\lambda\frac{\partial U_x}{\partial x} - 4R\tau_0\left(\frac{\partial^2 \xi_1}{\partial x^2} + R\frac{\partial^2 \xi_2}{\partial x^2}\right) = 0 \tag{53}$$

$$\begin{aligned} &\frac{4}{5}\rho R^2 \ddot{\xi}_1 + \frac{2}{3}\rho R^3 \ddot{\xi}_2 + (8\lambda + 2G)\xi_1 + R(9\lambda + 10G)\xi_2 \\ &+4\lambda\frac{\partial U_x}{\partial x} - 4R\tau_0\left(\frac{\partial^2 \xi_1}{\partial x^2} + R\frac{\partial^2 \xi_2}{\partial x^2}\right) = 0 \end{aligned} \tag{54}$$

It should be mentioned that Poisson's ratio effects are also included in derivation of the above governing equations. Moreover, different from the conventional high-order continuum theory, the current high-order model contains the parameters related to the strain-independent, the strain–dependant surface stress and intrinsic length scales, and thus can reflect size and surface dependent wave responses in the nanowire. As shown in Eq. (52), the effects of the strain-dependent surface stress upon the wave propagation can be predicted by considering different surface moduli $E_s$. For simplicity and clarity, we will focus on effects of the strain-independent surface stress upon the wave propagation by setting $E_s = 0$ in the study.

### 4.1.2 Flexural wave motion

Following a similar manner, a high-order continuum model will be formulated to analyze flexural wave propagation in nanowires to capture heterogeneous nanostructure effects. A coordinate system ($x$, $y$, $z$) will be adopted with the origin of the coordinate at the center of the cross section, where $x$ is the coordinate along the axis direction, and $y$ and $z$ are the coordinates along the cross-section directions. Based on the current high-order model for the flexural wave motion, local displacements can be approximated as

$$u_x = -z\Psi_1(x,t) - z^3\Psi_2(x,t),\ u_z = W_z(x,t) \tag{55}$$

where $\Psi_1(x,t)$ and $\Psi_2(x,t)$ are kinematic variables to capture local motion due to heterogeneity. The linearized strain-displacement relations are given by

$$\varepsilon_{xx} = -z\partial\Psi_1(x,t)/\partial x - z^3\partial\Psi_2(x,t)\partial x \tag{56}$$

$$\gamma_{xz} = -\Psi_1(x,t) - 3z^2\Psi_2(x,t) + \partial W_z(x,t)/\partial x \tag{57}$$

in which $\varepsilon_{xx}$ and $\gamma_{xz}$ are the normal strain and the transverse shear strain respectively. The isotropic constitutive equations of the nanowire are

$$\sigma_{xx} = E\varepsilon_{xx},\ \sigma_{xz} = \kappa G\gamma_{xz} \tag{58}$$

where $E$ and G are the Young's modulus and shear modulus, respectively, and $\kappa$ is the shear correction coefficient with circular cross section $\kappa = \left(6+12\nu+6\nu^2\right)/\left(7+12\nu+4\nu^2\right)$ (Kaneko, 1975), in which $\nu$ is the Poisson's ratio.

To consider the surface stress effects and follow the Trefftz's theory, the incremental deformation energy density $\Delta U$ can be obtained as

$$\Delta U = \left\langle \int_0^{\varepsilon_{xx}} \sigma_{xx} d\varepsilon_{xx} + \int_0^{\gamma_{xz}} \sigma_{xz} d\gamma_{xz} + \int_0^{\varepsilon_{xx}} \tau_e d\varepsilon_{xx} + \int_0^{\hat{\varepsilon}_{xx}} \tau_0 d\hat{\varepsilon}_{xx} - \int_0^{\varepsilon_{xx}} \tau_0 d\varepsilon_{xx} \right\rangle \tag{59}$$

where $\hat{\varepsilon}_{xx} = -z\frac{\partial\Psi_1}{\partial x} - z^3\frac{\partial\Psi_2}{\partial x} + \frac{1}{2}\left(z\frac{\partial\Psi_1}{\partial x}\right)^2 + z^4\frac{\partial\Psi_1}{\partial x}\frac{\partial\Psi_2}{\partial x} + \frac{1}{2}z^6\left(\frac{\partial\Psi_2}{\partial x}\right)^2 + \frac{1}{2}\left(\frac{\partial W_z}{\partial x}\right)^2$ is the Lagrangian stain component for the flexural wave motion. The kinetic energy density for flexural motion can be obtained as

$$T = \left\langle \frac{1}{2}\rho\left(\dot{u}_x^2 + \dot{u}_z^2\right) \right\rangle \tag{60}$$

Similarly, by applying the Hamilton's principle, equations of the flexural motion can be readily obtained as

$$\rho\ddot{W}_z + \kappa G\left(\frac{\partial\Psi_1}{\partial x} - \frac{\partial^2 W_z}{\partial x^2} + \frac{3}{4}R^2\frac{\partial\Psi_2}{\partial x}\right) - \frac{2\tau_0}{R}\frac{\partial^2 W_z}{\partial x^2} = 0 \tag{61}$$

$$\begin{aligned}&\rho R^2\ddot{\Psi}_1 + 4\kappa G\left(\Psi_1 - \frac{\partial W_z}{\partial x} + \frac{3}{4}R^2\Psi_2\right) - ER^2\left(\frac{\partial^2\Psi_1}{\partial x^2} + \frac{1}{2}R^2\frac{\partial^2\Psi_2}{\partial x^2}\right)\\ &+\frac{1}{2}\rho R^2\ddot{\Psi}_2 - 4R\left(\tau_0 + E_s\right)\frac{\partial^2\Psi_1}{\partial x^2} - 3R^3\left(\tau_0 + E_s\right)\frac{\partial^2\Psi_2}{\partial x^2} = 0\end{aligned} \tag{62}$$

$$\begin{aligned}&\rho R^4\ddot{\Psi}_2 + \frac{48}{5}\kappa G\left(\Psi_1 - \frac{\partial W_z}{\partial x} + \frac{3}{2}R^2\Psi_2\right) - \frac{8}{5}ER^2\left(\frac{\partial^2\Psi_1}{\partial x^2} + \frac{5}{8}R^2\frac{\partial^2\Psi_2}{\partial x^2}\right)\\ &+\frac{8}{5}\rho R^2\ddot{\Psi}_1 - \frac{48}{5}R\left(\tau_0 + E_s\right)\frac{\partial^2\Psi_1}{\partial x^2} - 8R^3\left(\tau_0 + E_s\right)\frac{\partial^2\Psi_2}{\partial x^2} = 0\end{aligned} \tag{63}$$

Similarly, the impacts of the strain-independent surface stress on the wave responses will be the focus for simplicity and clarity in the study by setting $E_s = 0$ .

### 4.2 Wave propagation and numerical simulation

By assuming the waveform $U = \bar{A}e^{ik(x-ct)}$ , $\xi_1 = \bar{B}e^{ik(x-ct)}$ , $\xi_2 = \bar{C}e^{ik(x-ct)}$ , and $W_z = \tilde{A}e^{ik(x-ct)}$ , $\Psi_1 = \tilde{B}e^{ik(x-ct)}$ , $\Psi_2 = \tilde{C}e^{ik(x-ct)}$ for corresponding longitudinal and flexural wave motion, where $k$ and $c$ denote wave number and phase velocity, respectively, the harmonic dispersion realtions of corresponding wave motion can be obtained (Song et al., 2009).

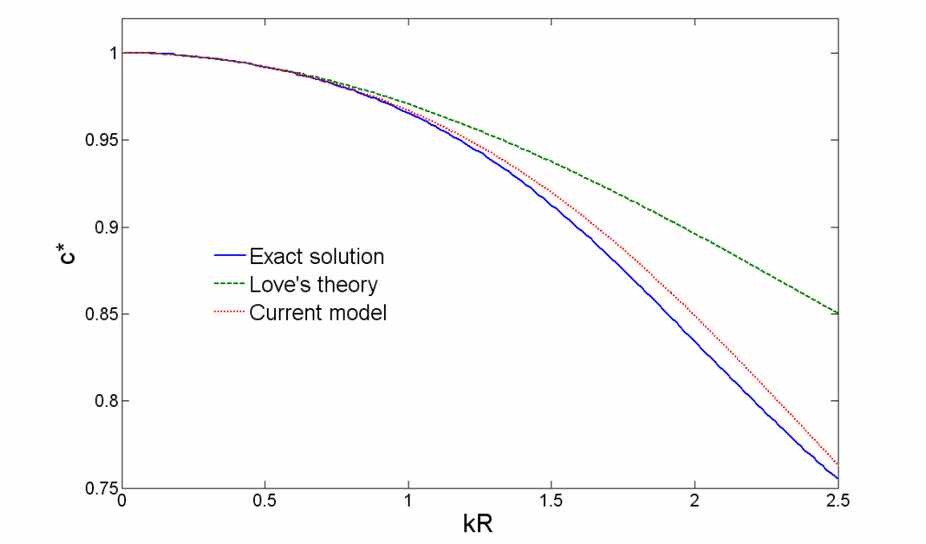


Fig. 8. The comparison of the nondimensional wave dispersion curves

The accuracy of the proposed model is discussed in Fig. 8 by the comparison of the longitudinal wave dispersion relations predicted from the current model and the love's theory (Achenbach, 1973) with that obtained from the exact solution, respectively. The exact solution is based on wave solution from the elasticity theory (Achenbach, 1973). In the example, surface effects are ignored by setting $\tau_0 = 0$ . The material parameters for the calculation are $E = 68.5GPa$ , $\nu = 0.35$ , $\rho = 2700Kg/m^3$ . The nondimensional wave velocity is defined as $c^* = c/c_0$ , with $c_0 = \sqrt{E/\rho}$ , and non-dimensional wave number $kR$ are used in this figure. It can be found that all models can give very good predictions of the longitudinal wave dispersion for the frequency range within $kR$<1.0. However, the dispersion curve from the love's theory deviates substantially from the exact curve for $kR$>1.0. The current model can still give a reasonable prediction even when the frequency becomes extremely high for example $kR$=2.5, which shows the accuracy of the proposed model to capture the heterogeneous nanostructure effects.

Surface stress effects upon longitudinal wave propagation in nanowire are depicted in Fig. 9. In the following simulation, the nondimensional strain-independent surface stress parameter is introduced by $\tau_0^* = \beta\tau_0/E$ , where $\beta$ is a constant coefficient for normalization

taken as $1\times10^{9}m^{-1}$ for the current case, and positive and negative values of surface stress parameter $\tau_0^*$, which physically denote surface tension and compression respectively, are selected. The material parameters used for the calculation are assumed to be $E=68.5GPa$, $\nu=0.35$, $\rho=2700Kg/m^3$ and $R$=3$nm$. It can be found that the longitudinal wave phase velocity increases with the increase of surface tension, however, wave phase velocity decreases with the increase of surface compression. As a result, if one employs the wave dispersion relation to determine nanowire's material properties ignoring surface effects ($\tau_0^*=0$), their values may be significantly underestimated or overestimated. It should be mentioned that the phase velocity size dependence can be different if different material and surface properties are under investigation.

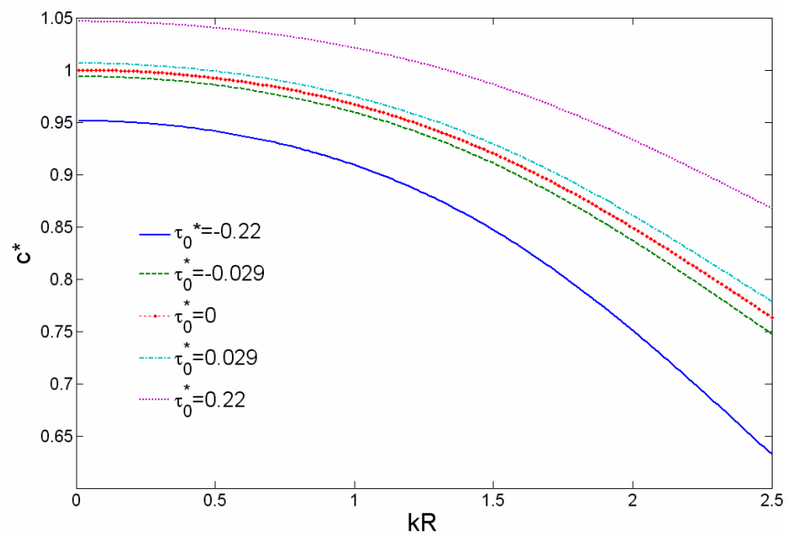


Fig. 9. Nondimensional longitudinal wave dispersion curves of the nanowire with different surface stresses

Size dependent effects of the nanowire upon longitudinal wave propagation are shown in Fig. 10 with the radius of nanowires being of 3, 10, 50 and 100$nm$ respectively. The material parameters for the calculation are assumed to be $E=68.5GPa$, $\nu=0.35$, $\rho=2700Kg/m^3$ and $\tau_0^*=0.22$. For the comparison, the wave dispersive result for $\tau_0^*=0$ is also depicted. It is well known that the dispersion relation does not alter with respect to the radius of the nanowire $R$ if surface effect is neglected ($\tau_0^*=0$), since the continuum mechanics cannot capture size effect of nanomaterials (Lim & He, 2004). However, by considering the surface stress effects in the current model, we can find that the phase wave velocity increases with decrease of the size of the nanowire under surface tension. It should be mentioned that the increase tendency of quasi-static phase velocity ($kR$ approaches zero) predicted by the proposed model has a very good agreement with the theoretical and experimental predictions about the Young's modulus of nanowires under surface tension (Wang & Li, 2008; Cuenot, et al. 2004). It is also noticed that the prediction about the phase

velocity, in which the Poisson's ratio effect related to the surface stress is only considered(Wu & Dzenis, 2006), is not in agreement with the results by the current model. It is also worth to point out that the size dependence of the longitudinal motion becomes even more evident with the increase of the wave frequency.

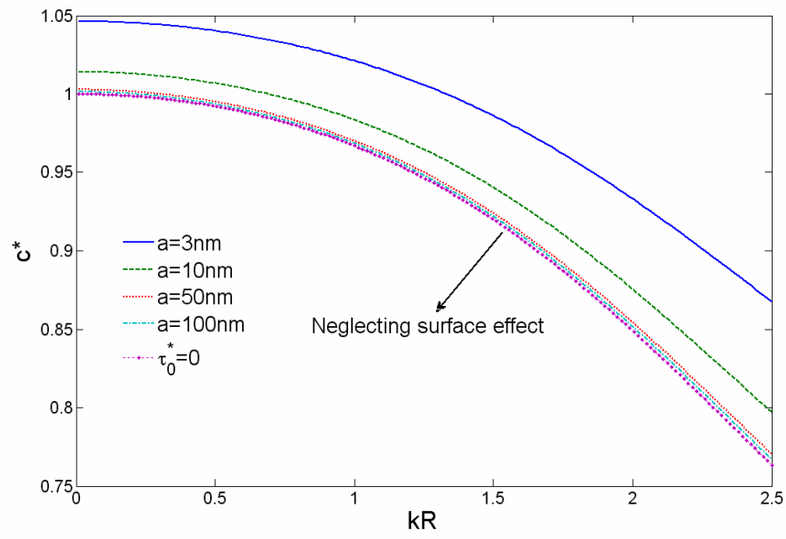


Fig. 10. Nondimensional longitudinal wave dispersion curves of the nanowire with different sizes

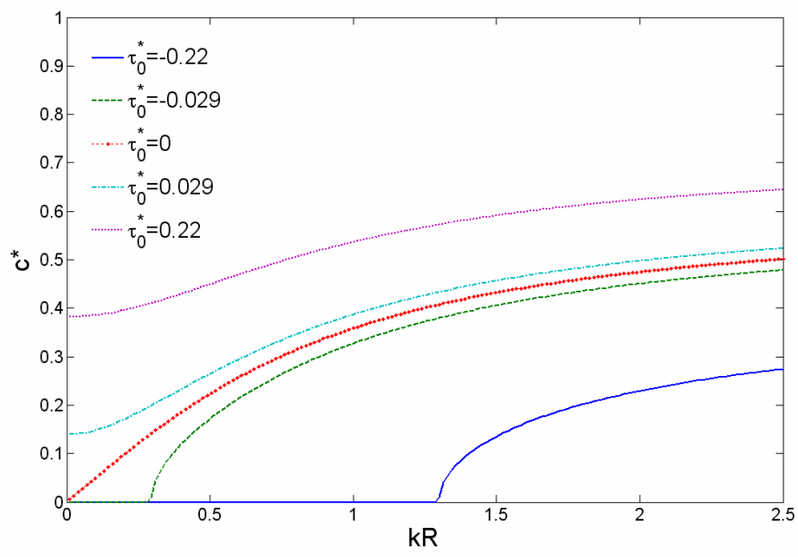


Fig. 11. Nondimensional flexural wave dispersion curves of the nanowire for different surface stresses

Fig. 11 shows surface stress effects upon flexural wave dispersion relations of nanowires. The material parameters are $E = 68.5GPa$, $\nu = 0.35$, $\rho = 2700Kg/m^3$ and $R$=3$nm$. Similarly, it can be found that the flexural wave phase velocity of the nanowire increases with the increase of the surface tension, while the phase velocity of the nanowire decreases with the increase of the surface compression. It is also of interest to notice that flexural stopping wave band can be observed in the nanowire subject to surface compression ($\tau_0^* < 0$), for example, the stopping wave band is 0<$kR$<0.28 for the nanowire under surface compression $\tau_0^* = -0.029$ and the stopping wave band is 0<$kR$<1.3 for $\tau_0^* = -0.22$.

Fig. 12 shows size dependent effects upon flexural wave propagation in the nanowire with radius of nanowires being of 3, 10, 50 and 100$nm$, respectively. The material parameters used in the calculation are $E = 68.5GPa$, $\nu = 0.35$, $\rho = 2700Kg/m^3$ and $\tau_0^* = 0.22$. For the comparison, wave dispersive curve for the nanowire without surface stress $\tau_0^* = 0$ is also included in the figure. Comparing the results with those in Fig. 10, similar size effects upon the flexural wave propagation can be observed with those in the longitudinal wave propagation. For example, the phase velocity for the nanowire with the radius being 3$nm$ is four times bigger than that for the nanowire with the radius being 50$nm$ when $kR$=0.

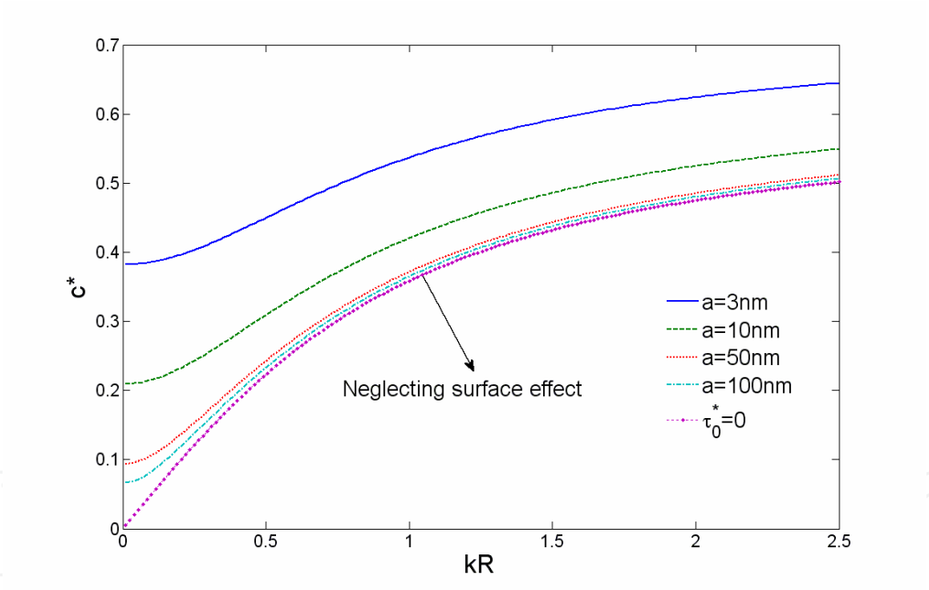


Fig. 12. Nondimensional flexural wave dispersion curves of the nanowire with different sizes

## 5. Conclusions

In this chapter, we develop a microstructure continuum theory to study wave propagation in the elastic media with different micro- or nano- structures. One of the main advantages of this approach is that the constitutive relations are derived explicitly from the properties and configuration of the microstructure and, theoretically, no additional experiments are

necessary. For different nanomaterials, we have demonstrated that microstructure continuum theories can be a good tool for modeling high-frequency wave propagation in nano-phononic crystals and ultra-thin films. A high-order continuum model including surface stress effects is also developed to study wave propagation in nanowires. In this model, surface stress effects are considered by using the incremental deformation theory. The accuracy of the proposed models is validated by numerical simulation. Some new physical wave phenomena related to the heterogeneous effects and surface stress effects on high-frequency wave propagation is discussed.

## 6. References

Achenbach, J. D. (1973). *Wave Propagation in Elastic Solids,* Elsevier, New York.

Achenbach, J. D.; Sun, C.T. & Herrmann, G. (1968). On the vibrations of a laminated body. *J. Appl. Mech. (Trans. ASME),* Vol. 35, pp. 689-696.

Biot, M. A. (1965). *Mechanics of Incremental Deformations,* Wiley, New York.

Chen, Y. & Lee, J. D. (2003a). Connecting molecular dynamics to micromorphic theory. (I). instantaneous and averaged mechanical variables. *Phys. A,* Vol. 322, pp. 359-376.

Chen, Y. & Lee, J. D. (2003b). Determining material constants in micromorphic theory through phonon dispersion relations. *Int. J. Eng. Sci.*, Vol. 41, pp. 871-886.

Cosserat, E. & Cosserat, F. (1909). *Theorie des Corps Deformables*, A. Hermann & Fils, Paris.

Craighead, H. G. (2000). Nanoelectromechanical system. *Science,* Vol. 290, No. 5496, pp. 1532-1535.

Cuenot, S.; Fre´tigny, C.; Demoustier-Champagne, S. & Nysten, B. (2004). Surface tension effect on the mechanical properties of nanomaterials measured by atomic force microscopy. *Phys. Rev. B,* Vol. 69, pp. 165410.

Eringen, A. C. (1999). *Microcontinuum field theories I: foundations and solids,* Springer Verlag, New York.

Feng, X. L.; He, R. R.; Yang, P. D. & Roukes, M. L. (2007). Very high frequency silicon nanowire electromechanical resonators. Nano Lett., Vol. 7, No. 7, pp. 1953-1959.

Ghatak, A. & Kothari, L. (1972). *An introduction to lattice dynamics,* Addison-Wesley.

Hernaandez, C. M.; Murray, T. W. & Krishnaswarmy S. (2002). Photoacoustic characterization of the mechanical properties of thin films. *Appl. Phys. Lett.*, Vol. 80, No. 4, pp. 691-693.

Huang, G. L. & Sun C. T. (2006a). A continuum model with microstructure for wave propagation in ultra-thin films. *Int. J. Solids Struct.,* Vol. 43, pp. 7104-7127.

Huang, G. L. & Sun C. T. (2006b). Modeling heterostructures of nano-phononic crystals by continuum model with microstructures. *Appl. Phys. Lett.,* Vol. 88, pp. 261908.

Huang, G. L. & Sun C. T. (2007). Continuum modeling of heterogeneous media with microstructures or nanostructures. *Phil. Mag. A*, Vol. 87, pp. 3689-3707.

Huang, G. L. & Sun C. T. (2008). A Higher-order continuum model for elastic media with multiphased microstructures. *Mech. Adv. Mater. Struct.,* Vol. 15, pp. 1-8.

Huang, G. L. & Song, F. (2008). High-frequency antiplane wave propagation in ultra-thin films with nanostructures. *Int. J. Solids Struct.,* Vol. 45, pp. 5368-5380.

Husain, A.; Hone, J.; Henk, W.; Postma, Ch.; Huang, X. M. H.; Drake, T.; Barbic, M.; Scherer, A. & Roukes, M. L. (2003). Nanowire-based very-high-frequency electromechanical resonator. *Appl. Phys. Lett.*, Vol. 83, No. 6, pp. 1240-1242.

Jin, Z. H.; Zhou, H. J.; Jin, Z. L.; Savinell, R. F. & Liu, C. C. (1998). Application of nano-crystalline porous tin oxide thin film for CO sensing. *Sensors and Actuators B: Chemical*, Vol. 52, pp. 188-194.

Kaneko, T. (1975). On Timoshenko's correction for shear in vibrating beams. *J. Phys. D Appl. Phys.,*Vol. 8, pp. 1927-1936.

Lim, C. W. & He, L. H. (2004). Size-dependent nonlinear response of thin elastic films with nano-scale thickness. *Int. J. Mech. Sci.,* Vol. 46, pp. 1715-1726.

Mindlin, R. D. (1964). Micro-Structure in linear elasticity. *Arch. Rat. Mech. Anal.,* Vol. 16, pp. 51-78.

Park, H. S. & Klein, P. A. (2008). Surface stress effects on the resonant properties of metal nanowires: The importance of finite deformation kinematics and the impact of the residual surface stress. *J. Mech. Phys. Solids*, Vol. 56, pp. 3144-3166.

Philip, J.; Hess, P.; Feygelson, T.; Butler, J. E.; Chattopadhyay, S.; Chen, K. H. & Chen, L. C. (2003). Elastic mechanical and thermal properties of nanocrystalline diamond films. *J. Appl. Phys.,* Vol. 93, No. 4, pp. 2164-2171.

Ramprasad, R. & Shi, N. (2005). Scalability of phononic crystal heterostructures. *Appl. Phys. Lett.,* Vol. 87, pp. 111101.

Sampathkumar, A.; Murray, T. W. & Ekinci, K. L. (2006). Photothermal operation of high frequency nanoelectormechanical systems. *Appl. Phys. Lett.,* Vol. 88, pp. 223104.

Schneider, D.; Witke, T.; Schwarz, T.; Schoneich, B. & Schultrich, B. (2000). Testing ultra-thin films by laser-acoustics. *Surf. Coat. Technol.,* Vol. 126, pp. 136-141.

Song, F.; Huang, G. L. & Varadan, V. K. (2010). Study of wave propagation in nanowires with surface effects by using a high-order continuum theory. *Acta Mech.,* Vol. 209, pp.129-139.

Song, F. & Huang, G. L. (2009). Modeling surface stress effects on bending behavior of nanowires: incremental deformation theory, *Phys. Lett. A,* Vol. 373, pp. 3969-3973.

Sun, C. T.; Achenbach, J. D. & Herrmann, G. (1968). Continuum theory for a laminated medium. *J. Appl. Mech. (Trans. ASME),* Vol. 35, pp. 467-475.

Sun, C. T. (1972). On the equations for a Timoshenko beam under initial stress. *J. Appl. Mech. (Trans. ASME),* Vol. 39, pp. 282-285.

Sun, C. T. & Zhang, H. T. (2003). Size-dependent elastic moduli of platelike nanomaterials. *J. Appl. Phys.,* Vol. 93, pp. 1212-1218.

Vollmann, J.; Profunser, D. M.; Meier, A. H.; Dobeli, M. & Dual, J. (2004). Pulse laser acoustics for the characterization of inhomogeneities at interfaces of microstructures. *Ultrasonics,* Vol. 42, pp. 657-663.

Wang, G. F. & Li, X. D. (2008). Predicting the Young's modulus of nanowires from first-principles calculations on their surface and bulk materials. *J. Appl. Phys.,* Vol. 104, pp. 113517.

Wu, X. F. & Dzenis, Y. A. (2006). Wave propagation in nanofibers. *J. Appl. Phys*., Vol. 100, pp. 124318.


**Wave Propagation in Materials for Modern Applications**

Edited by Andrey Petrin

ISBN 978-953-7619-65-7
Hard cover, 526 pages
**Publisher** InTech
**Published online** 01, January, 2010
**Published in print edition** January, 2010

In the recent decades, there has been a growing interest in micro- and nanotechnology. The advances in nanotechnology give rise to new applications and new types of materials with unique electromagnetic and mechanical properties. This book is devoted to the modern methods in electrodynamics and acoustics, which have been developed to describe wave propagation in these modern materials and nanodevices. The book consists of original works of leading scientists in the field of wave propagation who produced new theoretical and experimental methods in the research field and obtained new and important results. The first part of the book consists of chapters with general mathematical methods and approaches to the problem of wave propagation. A special attention is attracted to the advanced numerical methods fruitfully applied in the field of wave propagation. The second part of the book is devoted to the problems of wave propagation in newly developed metamaterials, micro- and nanostructures and porous media. In this part the interested reader will find important and fundamental results on electromagnetic wave propagation in media with negative refraction index and electromagnetic imaging in devices based on the materials. The third part of the book is devoted to the problems of wave propagation in elastic and piezoelectric media. In the fourth part, the works on the problems of wave propagation in plasma are collected. The fifth, sixth and seventh parts are devoted to the problems of wave propagation in media with chemical reactions, in nonlinear and disperse media, respectively. And finally, in the eighth part of the book some experimental methods in wave propagations are considered. It is necessary to emphasize that this book is not a textbook. It is important that the results combined in it are taken “from the desks of researchers“. Therefore, I am sure that in this book the interested and actively working readers (scientists, engineers and students) will find many interesting results and new ideas.

Slavka Krautzeka 83/A
51000 Rijeka, Croatia
Phone: +385 (51) 770 447
Fax: +385 (51) 686 166
www.intechopen.com

No.65, Yan An Road (West), Shanghai, 200040, China
中国上海市延安西路65号上海国际贵都大饭店办公楼405单元
Phone: +86-21-62489820
Fax: +86-21-62489821



IntechOpen

IntechOpen